Earth and Planetary Science Letters 568 (2021) 117052

Contents lists available at ScienceDirect

Earth and Planetary Science Letters

www.elsevier.com/locate/epsl

Using Zn and Ni behavior during magnetite precipitation in banded iron formations to determine its biological or abiotic origin

Xiaohua Han [a,b,c], Elizabeth J. Tomaszewski [a,1], Ronny Schoenberg [d], Kurt O. Konhauser [e], Matthieu Amor [f], Yongxin Pan [b,c], Viola Warter [a,d], Andreas Kappler [a], James M. Byrne [a,g,*]

[a] Geomicrobiology, Center for Applied Geosciences, University of Tübingen, Schnarrenbergstrasse 94-96, 72076 Tübingen, Germany
[b] Biogeomagnetism Group, Key Laboratory of Earth and Planetary Physics, Institute of Geology and Geophysics, Chinese Academy of Sciences, Beijing 100029, China
[c] College of Earth and Planetary Sciences, University of Chinese Academy of Sciences, Beijing 100049, China
[d] Isotope Geochemistry, Department of Geosciences, University of Tuebingen, Schnarrenbergstrasse 94-96, 72076 Tübingen, Germany
[e] Department of Earth and Atmospheric Sciences, University of Alberta, Edmonton, Alberta, Canada
[f] Aix-Marseille University, CNRS, CEA, UMR7265 Institute of Bioscience and Biotechnology of Aix-Marseille, CEA Cadarache, Saint-Paul-lez-Durance, F-13108, France
[g] School of Earth Sciences, University of Bristol, Wills Memorial Building, Queens Road, Bristol BS8 1RJ, United Kingdom

ARTICLE INFO

Article history:
Received 28 January 2021
Received in revised form 21 May 2021
Accepted 8 June 2021
Available online xxxx
Editor: F. Moynier

Keywords:
BIFs
mixed-valent iron oxide
zinc
nickel
Precambrian oceans

ABSTRACT

There is longstanding controversy about the genesis of magnetite in banded iron formations (BIFs), particularly concerning whether it is of abiogenic or biogenic origin. The composition of trace elements within magnetite produced by magnetotactic bacteria has been proposed as a promising marker for its biological origin; however further experimental evidence is required to investigate whether this also holds true for iron-metabolizing bacteria. Here, we compared the behavior of zinc (Zn) and nickel (Ni) in magnetite produced either abiogenically (ferrihydrite reacting with dissolved Fe^{2+}) or biogenically (ferrihydrite reacting with dissolved Fe^{2+} generated via the dissimilatory iron-reducing bacterium - DIRB - *Shewanella oneidensis* MR-1). These abiotic and biotic incubations were applied for transforming three ferrihydrite (Fh) substrates: (1) Control Fh without added trace elements; (2) Zn-coprecipitated ferrihydrite (ZnFh); and (3) Ni-coprecipitated ferrihydrite (NiFh) in both $NaHCO_3$ and HEPES buffer. X-ray diffraction revealed magnetite as the dominant transformation product for all reaction conditions, while siderite was only detected in experiments containing $NaHCO_3$ as buffer. Based on similar initial dissolved Ni and Zn concentrations, we found opposing behavior of Zn and Ni where Zn showed enrichment in abiogenic magnetite, while Ni was more enriched in biogenic magnetite. Combining supposed Zn and Ni concentrations in Precambrian seawater and magnetite mineral grains from three formations deposited at different ages (i.e. 3.75 Ga Nuvvuagittuq Supracrustal Belt, 2.45 Ga Weeli Wolli Iron Formation, and 1.88 Ga Sokoman Iron Formation), we reconstructed potential Zn and Ni partition coefficients between Precambrian seawater and magnetite minerals. The reconstructed potential Zn and Ni partition coefficients suggested that these magnetite minerals from three formations were abiogenic. These differing behaviors suggest the possibility of using Zn and Ni partition coefficient ratios as a means of determining the presence or absence of DIRB in the formation of ancient magnetite deposits.

1. Introduction

Banded iron formations (BIFs) are ancient sedimentary deposits of alternating silica-rich and iron-rich layers that were precipitated from seawater during the Archean and Proterozoic (Bekker et al., 2010; Konhauser et al., 2017). BIFs typically contain iron minerals with different oxidation states, including those comprised of only Fe(III) (e.g., hematite; Fe_2O_3), only Fe(II) (e.g., siderite; $FeCO_3$), and/or mixed valence phases (e.g., magnetite; $Fe(II)Fe(III)_2O_4$). It is generally agreed that the iron minerals in BIFs are not primary, but reflect both diagenetic and metamorphic transformation of one or more mineral precursors, such as ferrihydrite ($Fe(OH)_3$) (Konhauser et al., 2007; Sun et al., 2015), green

* Corresponding author at: School of Earth Sciences, University of Bristol, Wills Memorial Building, Queens Road, Bristol BS8 1RJ, United Kingdom.
E-mail address: james.byrne@bristol.ac.uk (J.M. Byrne).
[1] Current address: US Geological Survey, 3215 Marine St, Boulder CO 80303 USA.

https://doi.org/10.1016/j.epsl.2021.117052
0012-821X/

rust ($\left[Fe^{II}_{(6-x)}Fe^{III}_{x}(OH)_{12}\right]^{x+}\left[(A^{2-})_{x/2}\cdot yH_2O\right]^{x-}$ (where A denotes intercalated anions) (Halevy et al., 2017; Han et al., 2020a), as well as greenalite ($(Fe)_3Si_2O_5(OH)_4$) and siderite (Rasmussen and Muhling, 2018; Rasmussen et al., 2017).

It is currently thought that one of the main mechanisms of magnetite genesis in BIFs was partial reduction of ferric oxyhydroxide precursor minerals, such as ferrihydrite (reactions 1 and 2).

[1] $CH_3COO^- + 8Fe(OH)_3 \rightarrow 8Fe^{2+} + 2HCO_3^- + 15OH^- + 5H_2O$
[2] $8Fe^{2+} + 16Fe(OH)_3 + 16OH^- \rightarrow 8Fe_3O_4 + 32H_2O$

Reaction (1) is driven by dissimilatory iron-reducing bacteria (DIRB) that use ferric iron as an electron acceptor and organic compounds or H_2 derived from dead microbial cells as the electron donor to produce dissolved ferrous iron, which in turn reacts with extracellular ferrihydrite (reaction 2) to form magnetite (Konhauser et al., 2005; Posth et al., 2013a). The ecophysiological characteristics, stable isotope signature (Fe, C, O), and mineralogy of magnetite in BIFs support the important role of DIRB in BIF diagenesis (Johnson et al., 2003, 2005; Li et al., 2011; Vargas et al., 1998). Similarly, studies that applied pressure-temperature (P/T) burial simulations of ferrihydrite mixed with dead microbial biomass or glucose (as a proxy for biomass) showed that magnetite in BIFs could also have formed by thermochemical Fe(III) reduction under low P/T metamorphic conditions (Halama et al., 2016; Kohler et al., 2013; Posth et al., 2014, 2013b). Another biologically-mediated mechanism that leads to magnetite is via biologically controlled biomineralization by the so-called magnetotactic bacteria (MTB) (Blakemore, 1975). Unlike the magnetite formed via DIRB, the magnetite formed by magnetotactic bacteria is intracellular, has unique morphologies, is free from crystallographic defects, and shows limited incorporation of contaminant elements leading to its high chemical purity (Amor et al., 2020).

In addition to biotic transformations, abiotic transformation pathways of ferrihydrite into magnetite are also possible, such as the reaction of ferrihydrite with hot, Fe(II)-rich hydrothermal fluids (Klein, 2005). In this regard, Li et al. (2017) demonstrated experimentally that the reaction of Fe(II) with biogenic ferric iron under strict anoxic conditions and at temperatures $>50\,^{\circ}C$ leads to the formation of a metastable green rust phase which transformed into magnetite within hours. Alternatively, Rasmussen and Muhling (2018) and van Zuilen et al. (2002) argued that magnetite in BIFs formed through the replacement or thermal decomposition of siderite, and other ferrous-iron-bearing carbonates and silicates after burial (reaction 3 and 4).

[3] $3FeCO_3 + H_2O \rightarrow Fe_3O_4 + 3CO_2 + H_2$
[4] $6FeCO_3 \rightarrow 2Fe_3O_4 + 5CO_2 + C$

Given that magnetite has an inverse spinel structure with the general stoichiometry of $Fe^{2+}Fe^{3+}_2O^{2-}_4$, trace elements can partially substitute for Fe^{2+} or Fe^{3+} in this structure (e.g., Zn, Ni, Co, Cr, V, etc.), leading to magnetite with different characteristic trace elemental concentrations (Dupuis and Beaudoin, 2011; Nadoll et al., 2014). For example, Amor et al. (2015) compared the partitioning of 34 trace elements between magnetite (MTB and abiotic) and the aqueous solution from which it precipitated, and showed that the incorporation of most elements was at least 100 times lower in MTB magnetite compared to its abiotic counterpart. Indeed, Amor et al. (2015) showed that the biological or abiotic origin of magnetite could be determined from its trace element composition. The chemical purity of MTB magnetite was proposed to be generated by the selective internalization of iron for magnetite precipitation in these organisms, thus excluding distinct trace elements contained in the external solution. Such iron purification is not expected to occur in DIRB, as they precipitate magnetite in contact with the external solution. Additionally, the presence of microbial cells (e.g., DIRB) and microbially-derived organic material, such as extracellular polymeric substances (EPS) (Hao et al., 2016), may result in altered trace element incorporation into DIRB magnetic compared to its abiogenic counterpart.

However, little is known about such incorporation in the case of biological synthesis of magnetite by DIRB and abiotic reaction of Fe^{2+}_{aq} with ferrihydrite forming magnetite. In particular, zinc (Zn) and nickel (Ni) are incorporated into several specific Zn- and Ni-dependent enzymes, such as Zn metalloprotein and NiFe-hydrogenases (Althaus et al., 1999; Mulrooney and Hausinger, 2003). Therefore, the trace elements released by bacteria can then be associated with or incorporated into ferrihydrite before it is further transformed. Additionally, Zn- and Ni-enzymes are thought to have evolved early, as most of them are confined to anaerobic prokaryotes that were likely active on early Earth (Dupont et al., 2010; Zerkle et al., 2005).

In this study, we compared the partitioning of Zn and Ni between abiogenic or biogenic magnetite and the surrounding solution in order to determine whether such trace elements can be used as signatures for DIRB magnetite in BIFs. Magnetite was produced from the transformation of three ferrihydrite (Fh) substrates: (1) a control Fh which did not contain any added trace elements except from those already contained in the reagents; (2) Zn-coprecipitated ferrihydrite (ZnFh); and (3) Ni-coprecipitated ferrihydrite (NiFh). Abiogenic and biogenic transformation of Fh to magnetite was mediated by either addition of Fe^{2+}_{aq} (as $FeCl_2$) to Fh or by incubation with the DIRB *Shewanella oneidensis* strain MR-1, respectively. We monitored Fe(II) and Fe(III) concentrations in both aqueous and solid phases over time via chemical dissolution coupled to spectrophotometry, analyzed transformation products by X-ray diffraction, and quantified Zn and Ni associated with different Fe species (aqueous, adsorbed, colloidal, and Fe mineral fraction) by mass spectrometry.

2. Materials and methods

2.1. Preparation of Fh substrates

Control ferrihydrite without further addition of trace elements was precipitated by reaction of 99.999% pure $Fe(NO_3)_3 * 9H_2O$ (10 g) (Sigma-Aldrich, 7782-61-8) in 500 mL ultrapure water (Milli-Q) with KOH (Sigma-Aldrich, 99.99%) until pH 7.0 was reached (Raven et al., 1998). The material was centrifuged (7500 rpm; 10 min) and washed with ultrapure water (resistivity: 18.2 $M\Omega\ cm^{-1}$, Milli-Q™, Q-Gard® 2 Purification Cartridge) three times to remove nitrate ions. ZnFh and NiFh were synthesized following a similar approach with the addition of 16.6 mL of either 1000 mg/L Zn (EMD Millipore, 170369) or 1000 mg/L Ni (Sigma-Aldrich, CH-9471) ICP standard solutions into the $Fe(NO_3)_3 * 9H_2O$ solution before addition of KOH. In order to be comparable with the magnetite produced inside magnetotactic bacteria, the volumes of Zn and Ni ICP standard solutions were chosen to ensure that the ratios of Fh (dissolved Fe(III), ppm)/trace elements (ppm) were ~84 in accordance to Amor et al. (2015). The final Zn and Ni concentrations coprecipitated with Fh were determined by ICP-MS after dissolution with 6 M HNO_3 and further chemical treatment (see section 2.8).

2.2. Strains and medium

A *Shewanella oneidensis* MR-1 stock culture was streaked out on Luria-Bertani (LB) agar plates under oxic conditions. After incubation at 28 °C for 18 h in the dark, one colony was chosen to be transferred into 25 mL LB-medium and grown at 28 °C for 23 h.

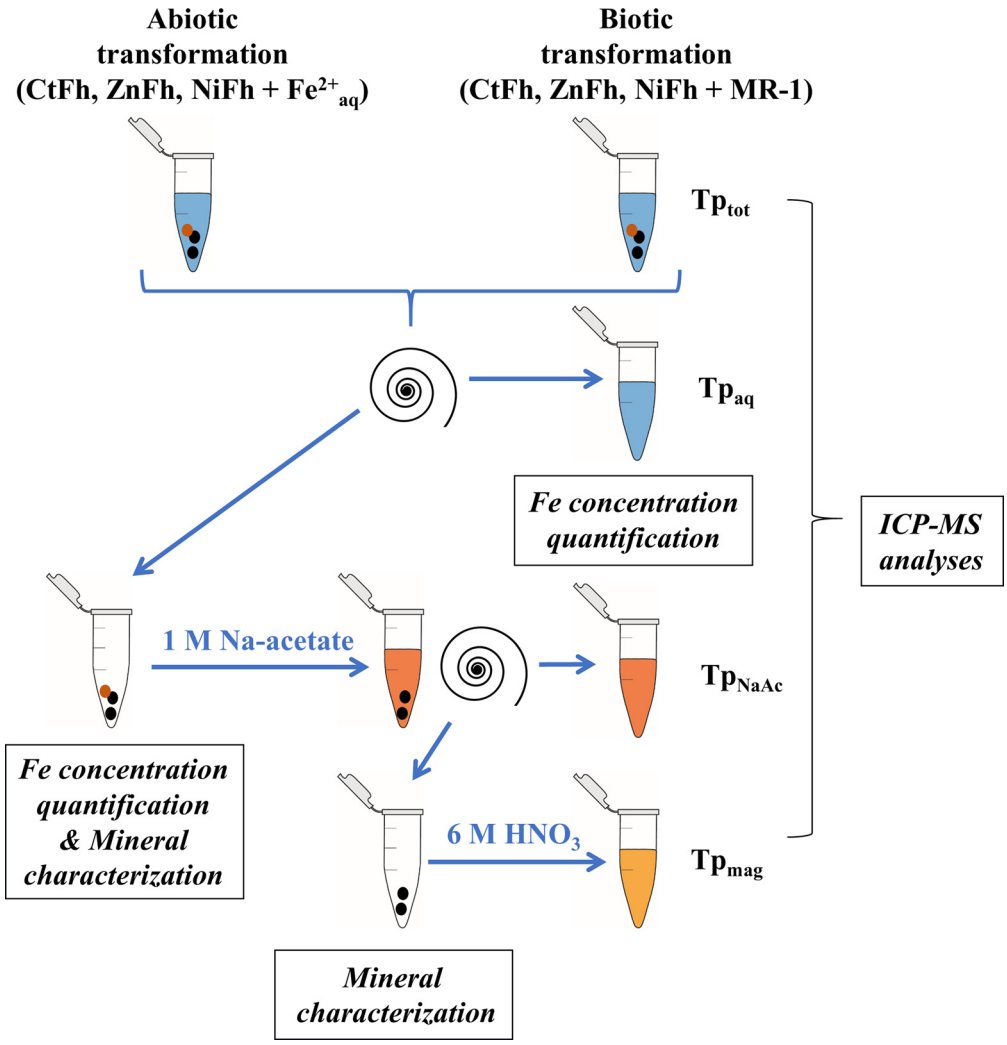

Fig. 1. Schematic summarizing the sampling strategy of the incubation experiments. Red dots and black dots correspond to siderite and magnetite, respectively. The spiral indicates a centrifugation step. Tp_{tot}, Tp_{aq}, Tp_{NaAc} and Tp_{mag} correspond to total transformation product, aqueous fraction, NaAc washing fraction and final precipitate fraction (should be pure magnetite) in transformation product, respectively. (For interpretation of the colors in the figure(s), the reader is referred to the web version of this article.)

There were 10 g tryptone, 6 g NaCl, 5 g yeast extract, 16 g agar (for LB-medium no agar added) per liter for LB agar plates and medium (Lies et al., 2005). Cells were harvested by centrifugation (7000 rpm, 10 min, 15 °C), washed and resuspended in 30 mM $NaHCO_3$ or HEPES (4-(2-hydroxyethyl)-1-piperazine-ethanesulfonic acid) buffer (pH 7.0) and transferred into bottles for the biotic experiments.

2.3. Optimization of the Fe^{2+}/Fh ratio and bacterial density for magnetite formation

Abiotic and biotic control Fh transformation experiments were applied to evaluate the optimum Fe^{2+}/Fh ratio and bacterial density needed for maximum abiogenic and biogenic magnetite formation, respectively (Piepenbrock et al., 2011). Abiotic Fh transformations were performed in 100 mL serum bottles with 50 mL of 30 mM anoxic $NaHCO_3$ buffer in which Fe^{2+}_{aq} was reacted with control Fh at Fe^{2+}/Fh ratios of 2:1 (24 mM $FeCl_2$ and 12 mM Fh) and 3:1 (36 mM $FeCl_2$ and 12 mM Fh), respectively. In biotic Fh transformation experiments, cell suspensions of *S. oneidensis* MR-1 with cell concentrations of 5×10^7 cells mL^{-1}, 7.5×10^7 cells mL^{-1}, 1×10^8 cells mL^{-1}, 2×10^8 cells mL^{-1}, 5×10^8 cells mL^{-1} and 7.5×10^8 cells mL^{-1} were used to reduce 12 mM Fh with 5 mM lactate as electron donor in 50 mL of 30 mM anoxic $NaHCO_3$ buffer.

2.4. Incubation experiments

The experimental methodology and the samples analyzed are summarized in Fig. 1. Given that there was likely a high concentration of HCO_3^- and CO_2 in ancient seawater and atmosphere (Konhauser et al., 2007; Ohmoto et al., 2004), we carried out several experiments with 30 mM bicarbonate buffer ($NaHCO_3$) to maintain environmental relevance. However, this can lead to the precipitation of siderite which could alter the trace metal incorporation into magnetite. Considering the $FeCO_3$ solubility product (K_{sp}) of $10^{-10.93}$ (Bénézeth et al., 2009), and the sum of HCO_3^- and CO_3^{2-} concentrations being 30 mM, $FeCO_3$ would precipitate when the Fe^{2+} concentration is higher than $3.3 \times 10^{-6.93}$ mM. XRD (X-ray diffraction) measurements of transformation products confirmed that there was siderite produced in the presence of $NaHCO_3$ buffer.

To evaluate the effect of siderite precipitation on trace element incorporation into magnetite, we ran parallel incubations using HEPES buffer. Given that there were no obvious differences between Fe concentration and mineral phases for abiotic control Fh transformation experiments with Fe^{2+}/Fh ratios of 2:1 and 3:1, a Fe^{2+}/Fh ratio of 2:1 (24 mM $FeCl_2$ and 12 mM Fh) was used for

Table 1
A summary for different Fe species from sequential extraction of transformation products from control Fh, ZnFh and NiFh substrates.

Transformation product	Label	Extraction, washing and separation method
Total	$CtTp_{tot}$, $ZnTp_{tot}$, $NiTp_{tot}$	6 M HNO_3
Aqueous fraction	$CtTp_{aq}$, $ZnTp_{aq}$, $NiTp_{aq}$	Centrifugation
NaAc washing fraction	$CtTp_{NaAc}$, $ZnTp_{NaAc}$, $NiTp_{NaA}$	1 M NaAc (pH = 5.0)
Final precipitate fraction (should be pure magnetite)	$CtTp_{mag}$, $ZnTp_{mag}$, $NiTp_{mag}$	6 M HNO_3

abiotic transformation of ZnFh and NiFh in 100-mL serum bottles with 50 mL of 30 mM anoxic $NaHCO_3$ buffer and HEPES buffer (pH 7.0). The resulting Fe(II) and Fe(III) concentration of the biotic control Fh transformation experiments using different cell numbers showed that when applying a cell number of 2×10^8 cells mL^{-1}, the final Fe(II)/Fe(III) ratio in the solid phase after ca. 10 days was ~0.5 which corresponds to stoichiometric magnetite. Therefore, *S. oneidensis* MR-1 at 2×10^8 cells mL^{-1} was added to a 12 mM Fh suspension with 5 mM lactate as electron donor in 30 mM anoxic $NaHCO_3$ or HEPES buffer (pH 7.0) for biotic transformation of ZnFh and NiFh. Triplicate experiments were used for Fe quantification and mineral characterization of final transformation products, and an additional two bottles were used for trace elements analyses. Control bottles containing neither Fe^{2+}_{aq} nor inoculum were included. Abiogenic and biogenic batch reactors were incubated at 28 °C in the dark for 17.3 days and 23.2 days, respectively.

2.5. Fe concentration quantification

For the Fe concentration analyses of the aqueous phases and solid phases, 1 mL of the samples was centrifuged at 13,400 rpm for 10 min (Fig. 1). The supernatant was stored in anoxic 1 M HCl to prevent Fe(II) oxidation (Porsch and Kappler, 2011). Solid pellets resulting from centrifugation were dissolved in anoxic 1 mL of 6 M HCl for 24 h and then diluted in anoxic 1 M HCl. All sampling and separation processes were done in an anoxic glovebox (100% N_2). Both Fe(II) and total Fe concentrations were quantified in the supernatant and solid phases using the spectrophotometric ferrozine assay (Stookey, 1970). Fe(III) concentrations were calculated as the difference between total Fe and Fe(II).

2.6. Sequential extraction of different Fe species for trace elements analyses

After ~20 days of incubation of the three Fh substrates in abiotic and biotic experiments, all Fh substrates were reduced or transformed to secondary minerals with no Fh detected using Mössbauer spectroscopy. Several Fe species were present, such as aqueous Fe, adsorbed Fe, Fe colloids and Fe minerals at the end of abiotic and biotic experiments (Table 1). To determine trace element concentrations associated with different Fe phases, sequential extractions were conducted using centrifugation and sodium acetate (NaAc) washing (Fig. 1). Bulk samples (2 mL) were removed with a 2-mL syringe as total Fe species of transformation products ($CtTp_{tot}$, $ZnTp_{tot}$, $NiTp_{tot}$). Additional 2 mL bulk samples were removed and centrifuged at 13,400 rpm for 10 min. The supernatant was collected as an aqueous fraction ($CtTp_{aq}$, $ZnTp_{aq}$, $NiTp_{aq}$). The pellet was then washed with anoxic 1 M NaAc (pH ~5.0) for 24 h in the dark for dissolving potential siderite. Washed samples were centrifuged (13,400 rpm for 10 min) and the supernatant was subsequently collected ($CtTp_{NaAc}$, $ZnTp_{NaAc}$, $NiTp_{NaAc}$). The final Fe precipitates after NaAc washing, which are supposed to be mainly magnetite ($CtTp_{mag}$, $ZnTp_{mag}$, $NiTp_{mag}$), were dissolved in 6 M HNO_3. Trace element concentrations for all fractions of final transformation products (total, aqueous, NaAc washing and final precipitate fraction) were analyzed. All sampling, washing and centrifugation steps for sequential extraction were conducted in an anoxic glovebox (100% N_2).

2.7. Mineral characterization

Given that ferrihydrite is short-range ordered and difficult to identify properly with XRD, starting Fh substrates and abiotic transformation products in preliminary experiments were analyzed by ^{57}Fe Mössbauer spectroscopy. 5 mL slurry samples were filtered (0.45 µm, nitrocellulose membrane) and the precipitates were sealed between Kapton tape in an anoxic glovebox (100% N_2). All samples were stored in anoxic sealed bottles at −20 °C until analysis. Samples were measured with a Mössbauer spectrometer (WissEL) with a ^{57}Co/Rh source at 77 K and 140 K. All spectra were fitted using the Voigt based fitting (VBF) routine in the Recoil software (University of Ottawa) (Rancourt and Ping, 1991). Total organic carbon (TOC) of both abiotic and biotic transformation products were quantified using a TOC analyzer (Model 2100S, Analytik Jena, Germany) after the samples were dried at 60 °C in an oven. Mineral phases of both abiotic and biotic transformation products, before and after treatment with NaAc, were dried in an anoxic glovebox and analyzed using a Bruker D8 Discover GADDS XRD^2-micro diffractometer with a Co-$K\alpha$ source at 30 kV and 30 mA. The total time measurement was 120 seconds at two detector positions, 15° and 40°, respectively (Berthold et al., 2009). The data were analyzed using the Jade 6.5 software.

2.8. Trace element analysis

All samples were digested in sealed, screw-top PFA beakers in 2 mL of 6 M HNO_3 solution on a hot plate at 120 °C for 24 h. The dissolved samples were evaporated and reacted with 200 µl of 30% H_2O_2 for three hours at room temperature to dissolve organic matter. Sample residues were dissolved in 2% ultrapure HNO_3 for 24 h and gravimetrically diluted to 2% HNO_3 stock solutions. The 2% HNO_3 used for dilution contained a mixture of ^{6}Li (3 ppb), In (1 ppb), Re (1 ppb), and Bi (1 ppb) to be used as an internal standard for trace element determinations with a Thermo Fisher Scientific iCAP Qc ICP-MS. The analytical procedure was similar to that described in Albut et al. (2018). Experiment sequences consisted of measurements of sample carrier solution (i.e. 2% HNO_3) blanks, calibration solutions prepared from different dilutions of the W-2a rock reference material, quality control rock reference materials (AGV-2, BIR-1, BHVO-2), and sample with unknown Zn and Ni concentrations. Repeated measurements of a monitor solution was analyzed between every 5–13 unknown sample for external drift correction after internal standard spike correction.

3. Results

3.1. Properties of ferrihydrite starting materials

Mössbauer spectra of all three Fh starting substrates showed doublets at 77 K with hyperfine parameters (Table S1, Fig. S1) that were indicative of ferrihydrite (Cornell and Schwertmann, 2003). There were no significant differences in the Mössbauer parameters between the three Fh substrates in the presence or absence of Zn and Ni.

Quantification of Zn and Ni in the three Fh substrates showed that despite minor Zn in control Fh (567 ppb) and NiFh (590 ppb), which probably stemmed from the chemical reagents used for Fh synthesis, the Zn concentration in ZnFh (1.1×10^5 ppb) was ~180 times higher than that in control Fh and NiFh. Similarly, there was extremely minor Ni in control Fh (118 ppb) and ZnFh (111 ppb),

while the Ni concentration in NiFh (1.0×10^5 ppb) was ~850 times higher than that in control Fh and ZnFh. The ratios of Zn/Fe for ZnFh and Ni/Fe for NiFh were determined to be 7.9×10^{-3} and 7.7×10^{-3}, respectively, while the ratios of Zn/Fe for NiFh, Ni/Fe for ZnFh, as well as both Zn/Fe and Ni/Fe for control Fh were $<0.1 \times 10^{-3}$ (Table S2).

3.2. Optimization of Fe^{2+}/Fh ratio and bacterial density for magnetite formation

We evaluated the optimal Fe^{2+}/Fh ratios and bacterial densities required for producing magnetite from ferrihydrite in both abiotic and biotic experiments. Iron speciation analyses showed that abiotic experiments with initial Fe^{2+}/Fh ratios of 2:1 and 3:1 exhibited no obvious differences in solid-phase Fe(II) or Fe(III) concentrations, with similar final Fe(II)/Fe(III) ratios of 1.1:1 after 14 days (Fig. S2). Mössbauer spectroscopic analysis of the final transformation products (Fig. S3) for the abiotic preliminary experiments suggested similar secondary minerals formed from control Fh, i.e., magnetite (76%) and siderite (18%). In the biotic experiments, the Fe(III) left in the solid phase (11.2-5.8 mM) and the Fe(II) produced (0.5-5.7 mM) decreased and increased with higher bacteria densities (from 5×10^7 to 7.5×10^8 cells mL^{-1}), respectively, suggesting that more Fh was reduced to Fe(II) with higher cell concentrations (Fig. S4). Solid phases with Fe(II)/Fe(III) of 0.5, and typical of stoichiometric magnetite, were observed only with a cell concentration of 2×10^8 cells mL^{-1}.

3.3. Characterization of Fh transformation mineral products

XRD results of solid mineral products before (gray lines) and after Na-acetate extraction (black lines) are shown in Fig. 2. Both magnetite and siderite were identified in the mineral products obtained from all three Fh starting substrates in the abiotic experiments with $NaHCO_3$ buffer. In the corresponding biotic experiments with $NaHCO_3$ buffer, magnetite was identified in setups with all three Fh substrates together with minor patterns stemming from short-range ordered minerals which match goethite (α-FeOOH) as the transformation product. Siderite was also observed in the XRD pattern obtained for the mineral products from control Fh incubated in the biotic $NaHCO_3$ setup. In abiotic experiments with HEPES buffer, magnetite was identified but no siderite was observed. In addition to magnetite signals, some minor reflections were present in the abiotic HEPES experiments with ZnFh and NiFh, which we interpret to stem from goethite. In contrast, in the biotic experiments with HEPES buffer, magnetite was the only transformation product for all three Fh substrates.

In order to quantify the trace element content of the magnetite in setups where both siderite and magnetite were formed, we applied a sodium acetate (NaAc) extraction to remove the siderite from the solid phases. A comparison of X-ray diffractograms of the mineral products before and after NaAc extraction (Fig. 2) revealed that the siderite reflections were almost entirely removed in the extracted samples. Additionally, the XRD results showed some NaAc in all NaAc-extracted samples which originated from the sample preparation. Detailed information of the analyses of mineral products for the three Fh substrates are given in Table S3.

3.4. Ferrihydrite reduction and transformation in abiotic and biotic experiments using $NaHCO_3$ and HEPES buffers

Variations of Fe^{2+}_{aq} and solid-phase Fe(II)/Fe(III) ratios for both abiotic and biotic transformation products were followed to determine the rate and extent of Fh reduction and magnetite formation (Fig. 3). No Fe^{3+}_{aq} was detected in any experiment at any time point. Detailed data are provided in the Supporting Information.

In the abiotic Fh transformation experiments with HEPES buffer, 4.10-4.26 mM Fe^{2+}_{aq} were removed from the aqueous phase for all three Fh substrates after 17.3 days of incubation (Fig. 3 (a)), presumably through adsorption and reaction with Fh. By comparison, over the same time period of 17.3 days, the abiotic transformation experiments with $NaHCO_3$ buffer resulted in a removal of 12.94-13.10 mM Fe^{2+}_{aq} from the aqueous phase. The higher removal of Fe^{2+}_{aq} in the abiotic $NaHCO_3$ experiments is likely due to precipitation of $FeCO_3$ in addition to adsorption and reaction of Fe^{2+}_{aq} with Fh (see above, and the mineralogical characterizations). The corresponding Fe(II)/Fe(III) ratios in the solid phase after 17.3 days of incubation for the three Fh substrates in $NaHCO_3$ buffer conditions (1.09-1.35) were higher than in HEPES buffer (0.30-0.37) (Fig. 3 (b)), again in good agreement with the presence of siderite precipitated from $NaHCO_3$. Additionally, the Fe(II)/Fe(III) ratios in the solids at the first measured time point (0.5 h) were ~0.2 and ~0.4 (i.e. non-zero) for the three Fh substrates in HEPES and $NaHCO_3$ buffers, respectively, suggesting that adsorption of Fe^{2+}_{aq} to Fh occurred almost immediately after the start of the experiment.

In the biotic transformation experiments, *S. oneidensis* MR-1 reduced Fh to Fe(II). Consequently, the Fe(II) was either released to the supernatant as Fe^{2+}_{aq}, associated with Fh, or reacted with CO_3^{2-} from the buffer to form siderite. The aqueous Fe^{2+}_{aq} concentrations after 23.2 days of incubation of the three Fh substrates were higher in HEPES buffer (0.46-1.15 mM) than in $NaHCO_3$ buffer (0.03-0.23 mM) (Fig. 3 (c)). Similarly, solid-phase Fe(II) concentrations after 23.2 days were higher for all three Fh substrates incubated in HEPES buffer (3.9-4.1 mM) than in $NaHCO_3$ buffer (2.54-3.9 mM) (Fig. 3 (d)), implying that *S. oneidensis* MR-1 reduced more Fh to Fe(II) in HEPES buffer than in $NaHCO_3$ buffer. Correspondingly, after 23.2 days of incubation the solid-phase Fe(II)/Fe(III) ratios for all three Fh substrates were higher in HEPES buffer (0.43-0.56) than in $NaHCO_3$ buffer (0.21-0.38).

At the end of biotic experiments, more Fe^{2+}_{aq} was released by *S. oneidensis* MR-1 from incubations containing control Fh (0.23 mM and 1.15 mM in $NaHCO_3$ and HEPES buffer, respectively) than from ZnFh (0.03 mM and 0.7 mM in $NaHCO_3$ and HEPES buffer, respectively) and NiFh (0.05 mM and 0.46 mM in $NaHCO_3$ and HEPES buffer, respectively). The solid-phase Fe(II)/Fe(III) ratios for control Fh in HEPES buffer (0.56) were also higher than for ZnFh (0.44) and NiFh (0.43), while the solid-phase Fe(II)/Fe(III) ratio for control Fh in $NaHCO_3$ buffer (0.38) was similar with that for NiFh (0.37), but higher than that for ZnFh (0.21).

3.5. Zn and Ni partitioning between magnetite and the precipitation solution

Zn and Ni concentrations in the different fractions of transformation products are shown for both abiotic and biotic experiments in Table S2. Given there was no Fh detected by Mössbauer spectroscopy, we assume that all Fh was reduced or transformed to secondary minerals. During Fh reduction and dissolution, Zn and Ni were released into solution and subsequently incorporated into secondary minerals or adsorbed on cell surface. Both Zn/Fe and Ni/Fe were lower in all fractions of the abiotic compared to the biotic transformation products from ZnFh and NiFh. This is due to the dilution of the Zn and Ni concentration by the addition of Fe^{2+}_{aq} in abiotic setups which contained Fe, but no Zn or Ni. For abiogenic and biogenic magnetite, we described Zn and Ni partitioning between magnetite and residual solution using the partition coefficient (K_i^{Zn} and K_i^{Ni}) normalized to iron:

$$K_i^{Zn} = \frac{[Zn]_{magnetite}/[Zn]_{solution}}{[Fe]_{magnetite}/[Fe]_{solution}} \quad (1)$$

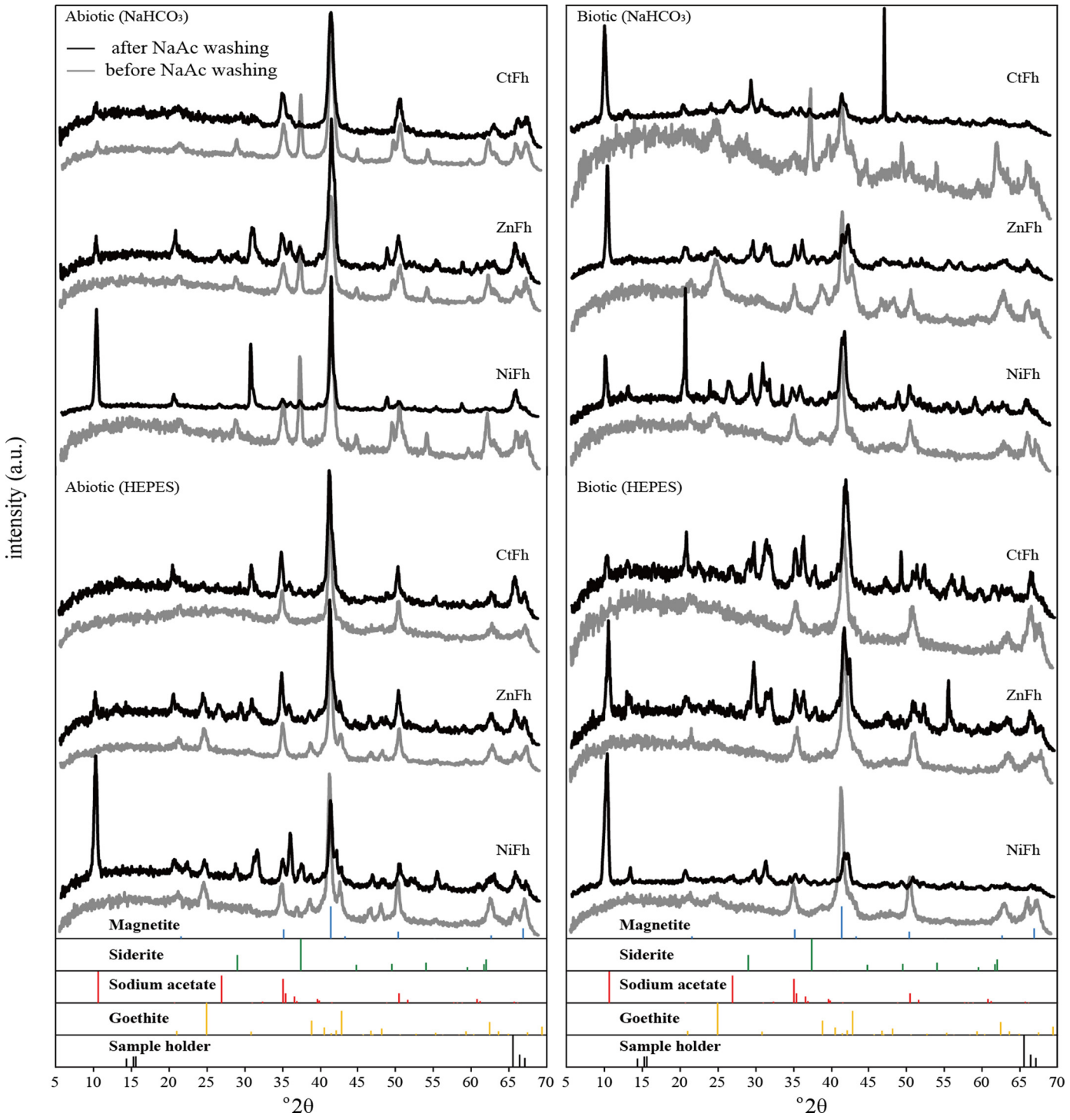

Fig. 2. X-ray diffractograms of solid mineral products transformed from three ferrihydrite substrates control Fh, ZnFh and NiFh under abiotic and biotic reductive conditions in $NaHCO_3$ and HEPES buffer. Gray lines and black lines are solid mineral products before and after sodium acetate (NaAc) extraction, respectively.

$$K_i^{Ni} = \frac{[\mathrm{Ni}]_{\mathrm{magnetite}}/[\mathrm{Ni}]_{\mathrm{solution}}}{[\mathrm{Fe}]_{\mathrm{magnetite}}/[\mathrm{Fe}]_{\mathrm{solution}}} \quad (2)$$

where i is A and B indicating abiogenic magnetite and biogenic magnetite, respectively. Rather than low or high levels of Zn and Ni impurities in magnetite, which directly depend on the initial Zn and Ni concentrations, the important point is to determine whether differential incorporation of Zn and Ni into magnetite exists between the abiotic and DIRB formation pathways. Thus, we used partition coefficients (K_i^{Zn} and K_i^{Ni}) to determine the origin of magnetite based on their Zn and Ni fingerprints. Here, the partition coefficient thus describes the affinity of Zn and Ni for magnetite in both precipitation conditions. Therefore, partition coefficients reflect the relative enrichment of Zn and Ni in magnetite compared to iron: if $K = 1$, Zn and Ni show the same partitioning between magnetite and solution as iron; if $K > 1$, Zn and Ni are enriched in magnetite relative to iron, whereas $K < 1$ corresponds to a depletion of Zn and Ni in magnetite relative to iron.

Partition coefficients of Zn and Ni between magnetite and solution for abiogenic and biogenic magnetite transformed from control Fh, ZnFh and NiFh substrates are reported in Table 2. For abio-

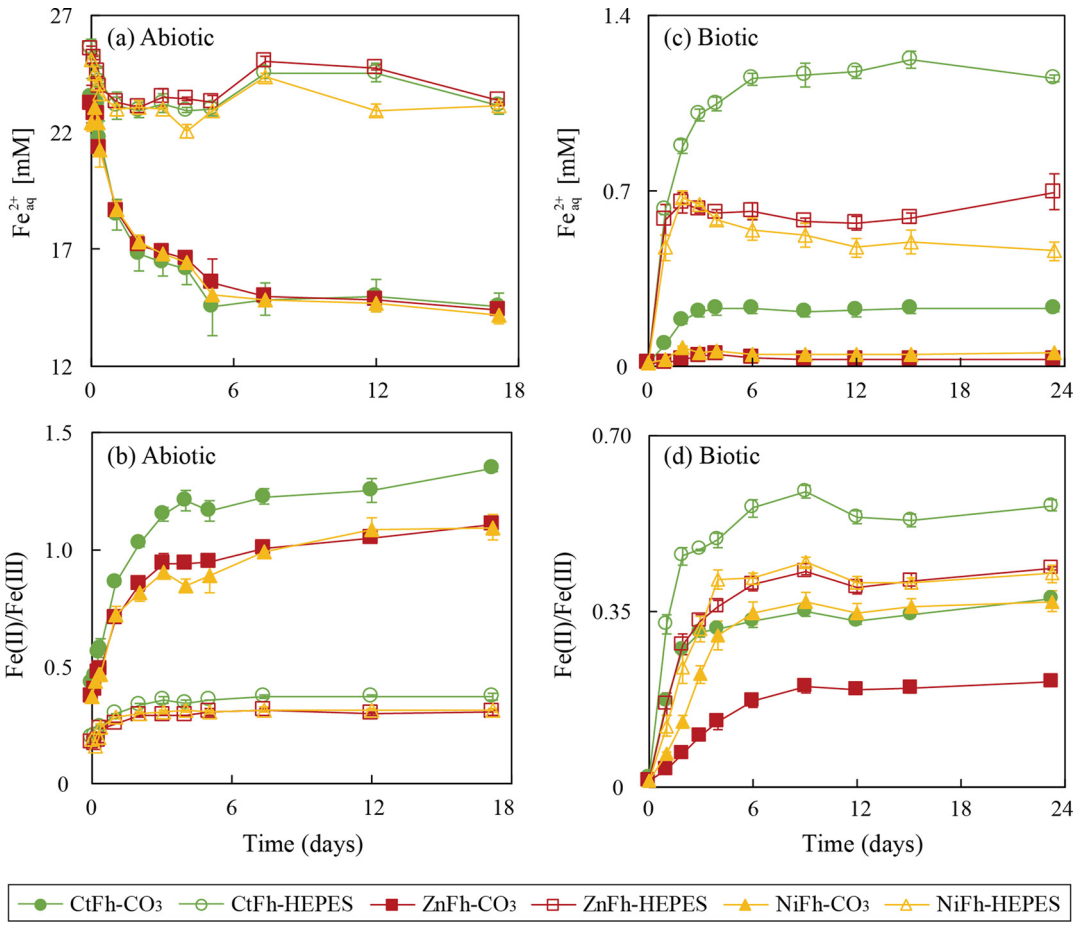

Fig. 3. Ferrihydrite transformation promoted abiotically by added Fe^{2+}_{aq} or biotically by the DIRB *S. oneidensis* MR-1, respectively. (a) and (c) are Fe^{2+}_{aq} concentrations in abiotic and biotic transformations of ferrihydrite; (b) and (d) are solid-phase Fe(II)/Fe(III) ratios over time in abiotic and biotic transformation of ferrihydrite. Error bars indicate the range of triplicate culture bottles. Bars not visible are smaller than the symbols.

Table 2
Zn and Ni partition coefficient (K_i^{Zn} and K_i^{Ni}) between magnetite and solution (normalized to iron, see Eq. (1) and Eq. (2)) for abiogenic and biogenic magnetite transformed from control Fh, ZnFh and NiFh substrates, respectively. Since Ni concentration for biogenic magnetite transformed from control Fh with HEPES buffer was 0, there was no K_B^{Ni} value for this magnetite.

Magnetite		K_i^{Zn}	K_i^{Ni}	K_i^{Zn}/K_i^{Ni}	K_A^{Zn}/K_B^{Zn}	K_A^{Ni}/K_B^{Ni}
control Fh transformation	Abiogenic ($NaHCO_3$)	1.09	0.71	1.53	99.38	11.93
	Biogenic ($NaHCO_3$)	0.01	0.06	0.18		
	Abiogenic (HEPES)	3.48	0.17	20.63	19.15	-
	Biogenic (HEPES)	0.18	-	-		
ZnFh transformation	Abiogenic ($NaHCO_3$)	5.58	0.52	10.78	248.18	22.89
	Biogenic ($NaHCO_3$)	0.02	0.02	0.99		
	Abiogenic (HEPES)	7.33	0.33	22.53	12.70	0.10
	Biogenic (HEPES)	0.58	3.21	0.18		
NiFh transformation	Abiogenic ($NaHCO_3$)	0.28	0.45	0.63	10.64	0.93
	Biogenic ($NaHCO_3$)	0.03	0.48	0.05		
	Abiogenic (HEPES)	1.94	0.32	6.02	33.55	1.40
	Biogenic (HEPES)	0.06	0.23	0.25		

genic magnetite, K_A^{Zn} ranged from 0.28 to 7.33; while K_A^{Ni} values show narrower variations and lower element incorporations (0.17-0.71). Most K_A^{Zn}/K_A^{Ni} ratios were >1 (Table 2), except for K_A^{Zn}/K_A^{Ni} (0.63) of the magnetite transformed from NiFh in $NaHCO_3$ buffer. This shows that Zn was therefore more enriched in abiogenic magnetite than Ni. Both K_B^{Zn} (0.01-0.18) and K_B^{Ni} (0.02-0.48) values for biogenic magnetite show much narrower variations, except for the magnetite transformed from ZnFh in HEPES buffer (K_B^{Zn}, 0.58; K_B^{Ni}, 3.21). Additionally, all K_B^{Zn}/K_B^{Ni} ratios were <1 (Table 2), indicating that Ni was more enriched in biogenic magnetite than Zn.

Comparing abiogenic and biogenic magnetite, all ratios between K_A^{Zn} and K_B^{Zn} were >1, especially for the magnetite transformed from ZnFh in $NaHCO_3$ buffer which was 248.18, indicating that Zn was up to ~250 times more enriched in abiogenic magnetite than in biogenic magnetite. For Ni, the ratios between K_A^{Ni} and K_B^{Ni} (11.93 and 22.89) of magnetite transformed from control Fh and ZnFh in $NaHCO_3$ buffer were >1, and while that of magnetite transformed from ZnFh in HEPES buffer was <1 (0.10), that of magnetite transformed from NiFh in both $NaHCO_3$ and HEPES buffer were close to 1 (0.93 and 1.40).

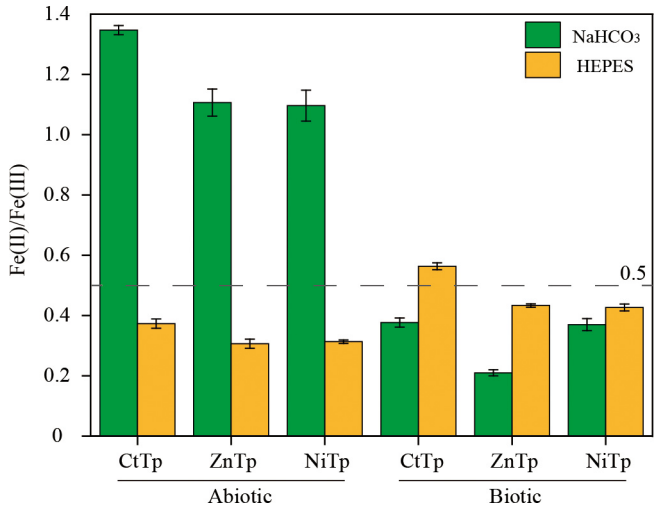

Fig. 4. Solid-phase Fe(II)/Fe(III) ratios in the transformation products (CtTp, ZnTp and NiTp) from three ferrihydrite substrates reduction promoted by Fe^{2+}_{aq} or Fe(III)-reducing bacteria *S. oneidensis* MR-1 in $NaHCO_3$ buffer (green color) and HEPES buffer (yellow color), respectively. The dashed line indicates a stoichiometric Fe(II)/Fe(III) value of 0.5 as present in magnetite with an ideal Fe(II):Fe(III) ratio of 1:2.

4. Discussion

4.1. Effect of co-precipitated trace elements and buffer on Fh reduction

As shown in Fig. 4, under both abiotic and biotic reduction conditions, the Fe(II)/Fe(III) ratios in the solid phase for the control Fh were higher than that of ZnFh and NiFh irrespective of whether they were precipitated in $NaHCO_3$ or HEPES buffer. These results suggest that more Fe(II) adsorbed and reacted with control Fh than with ZnFh and NiFh. Magnetite forms via dissolution of Fh and subsequent re-precipitation, via solid-state conversion of Fh, and/or a combination of both (Cornell and Schwertmann, 2003; Hansel et al., 2005). For these two pathways, the adsorption of Fe(II) to Fh is necessary to induce electron transfer and drive mineral transformation (Jolivet et al., 1992; Piepenbrock et al., 2011; Xiao et al., 2018). Therefore, the presence of coprecipitated Zn and Ni in Fh partially occupied adsorption sites, resulting in less Fe(II) adsorbed.

Apart from the changes related to the trace metal content, the buffer system used for the incubation experiments also altered the overall geochemistry. For the abiotic experiments (Fig. 4), the Fe(II)/Fe(III) ratios in the solid phase were much higher when formed in $NaHCO_3$ instead of HEPES buffer. However, the substantial increase of Fe(II)/Fe(III) ratios did not only correspond to faster Fh reduction, but also reflected the reaction between Fe^{2+}_{aq} with CO_3^{2-} from the $NaHCO_3$, leading to the precipitation of $FeCO_3$. Conversely, for biotic experiments (Fig. 4), the Fe(II)/Fe(III) ratios in the solid phase were lower in incubations containing $NaHCO_3$ instead of HEPES buffer. We postulate that the reasons for these lower Fe(II)/Fe(III) ratios in $NaHCO_3$ buffer include: (i) the precipitation of $FeCO_3$ on the surface of Fh resulting in passivation of the Fh surface layer which inhibits further reaction; (ii) the precipitation of $FeCO_3$ on the surface of bacterial cells causing less Fe(II) to be produced; and/or (iii) DIRB *S. oneidensis* MR-1 having a lower metabolic rate in $NaHCO_3$ buffer than in HEPES buffer, resulting in less Fe(II) production and thus lower Fe(II)/Fe(III) ratio.

4.2. Abiotic and biotic magnetite formation

Given that two mineral phases, namely siderite and magnetite, precipitated in the presence of $NaHCO_3$ buffer, both minerals contributed to the resulting Fe(II)/Fe(III) ratio of the solid phase. However, since magnetite was the only transformation product from Fh in HEPES buffer (based on XRD results), the Fe(II)/Fe(III) ratios in the solid phase produced in HEPES buffer only reflects the transformation rate of Fh to magnetite. As shown in Fig. 3, solid-phase Fe(II)/Fe(III) ratios for all three Fh substrates promoted by Fe^{2+}_{aq} in HEPES buffer reached a plateau within 2 days and increased by an average rate of 0.14-0.17 day^{-1}. This is much quicker than that promoted by *S. oneidensis* MR-1 which reached a plateau in 9 days and increased by an average rate of 0.05-0.07 day^{-1}. These results indicate that initial Fe^{2+}_{aq} concentration played a dominant role in the rate of magnetite formation from Fh, which is consistent with previous studies on Fe^{2+}_{aq} and DIRB-induced transformation of Fh (Dippon et al., 2015; Han et al., 2020b; Xiao et al., 2018).

Interestingly, the final solid-phase Fe(II)/Fe(III) ratios for all three Fh substrates promoted by Fe^{2+}_{aq} were 0.30-0.37, i.e. lower than that (0.43-0.56) promoted by *S. oneidensis* MR-1 in HEPES buffer. Previous studies on cation site occupancy in magnetite with *L*-edge X-ray magnetic circular dichroism (XMCD) also found that the biogenic magnetite produced by *G. sulfurreducens* and *S. oneidensis* showed a small excess (between 0.01–0.04) of Fe cations present as Fe^{2+} in octahedral sites (Coker et al., 2007, 2008). This work suggests that in general the biogenic magnetite was more reduced than abiogenic magnetite or that there was more Fe(II) adsorbed on the biogenic magnetite since bacteria and associated biomass (such as EPS) that were present could adsorb Fe(II) in the biotic experiments. This reasoning might also explain the differences observed in Fe(II)/Fe(III) ratios in magnetite formed from incubations containing $NaHCO_3$ instead of HEPES buffer.

4.3. Zn and Ni patterns of abiogenic versus biogenic magnetite

The direct comparison between Zn and Ni partitioning into abiogenic and biogenic magnetite reveals that Zn was more enriched in abiogenic magnetite (the ratio between Zn and Ni partition coefficient in abiogenic magnetite as high as ~22) while Ni was more enriched in biogenic magnetite (the ratio between Zn and Ni partition coefficient in biogenic magnetite was as low as 0.05). With regard to the effect of the initial trace element concentration in ferrihydrite substrates on Zn and Ni partitioning, Zn was more enriched in abiogenic magnetite than in biogenic magnetite, no matter whether magnetite was precipitated from ferrihydrite substrates with lower (~600 ppb) or higher (1.1×10^5 ppb) initial Zn concentration (Fig. 5). While there were obvious differences of Ni enrichment between abiogenic and biogenic magnetite (K_A^{Ni}/K_B^{Ni}) which precipitated from ferrihydrite substrates with lower initial Ni concentration (~100 ppb), the Ni enrichment difference between abiogenic and biogenic magnetite (K_A^{Ni}/K_B^{Ni}) which precipitated from ferrihydrite substrates with higher initial Ni concentration (1.0×10^5 ppb) were similar. We consider one reason which might have resulted in different partitioning of Zn and Ni into abiogenic and biogenic magnetite to be the different preference of Zn and Ni for tetrahedral sites or octahedral sites. Previous studies demonstrated that Ni^{2+} ions tend to substitute into octahedral sites while Zn^{2+} ions tend to substitute into tetrahedral sites (Coker et al., 2008; Schiessl et al., 1996). The final solid-phase Fe(II)/Fe(III) ratios with HEPES buffer likely reflect the actual Fe(II)/Fe(III) ratios of magnetite, which showed the average final solid-phase Fe(II)/Fe(III) ratios of abiogenic and biogenic magnetite were 0.33 and 0.47 which are lower than stoichiometric magnetite (i.e. 0.5), indicating there were less Fe^{2+} in octahedral sites compared with Fe^{3+} in tetrahedral sites. Therefore, there were less octahedral sites for Ni^{2+} ions substituting while more tetrahedral sites for Zn^{2+} ions substituting.

In this study, both abiogenic and biogenic magnetite have different trace metal partitioning compared to that in Amor et al. (2015), with the possible reasons discussed below. In the characterization of the chemical composition of magnetite produced

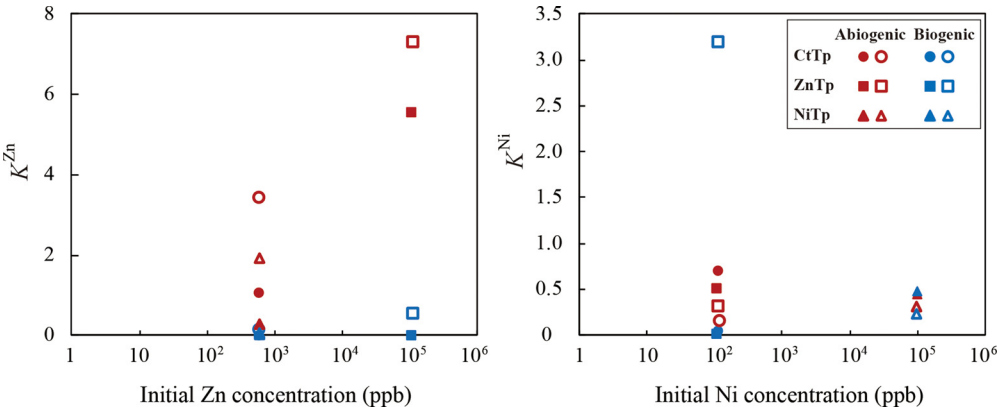

Fig. 5. Zn (K^{Zn}) and Ni (K^{Ni}) partition coefficients of magnetite products v.s. initial Zn and Ni concentrations of ferrihydrite substrates. Filled symbols indicate magnetite precipitated in $NaHCO_3$ buffer, while open symbols stand for magnetite precipitated in HEPES buffer, respectively.

by magnetotactic bacteria (Amor et al., 2015), the incorporation of both Zn and Ni was lower in biogenic magnetite than in abiogenic magnetite. For abiogenic magnetite, Zn and Ni partition coefficients normalized to iron were 0.02 and 0.2; for biogenic magnetite, Zn and Ni partition coefficients were 7×10^{-4} and 9×10^{-4} in their study. These partition coefficients were much lower than the Zn and Ni partition coefficients here, especially for the biogenic magnetite which further supports the high chemical purity of MTB magnetite. In the initial study of Amor et al. (2015), the abiogenic magnetite was synthesized from co-precipitation of Fe^{3+} and Fe^{2+} ions. In our study, the abiogenic magnetite transformed from Fh either via dissolution of Fh and subsequent re-precipitation, or most likely via solid-state conversion of Fh induced by the Fe^{2+} which leads to the trace elements staying in the transformation products. For the biogenic magnetite, the results presented in our study focus on a very different mechanism for magnetite formation, i.e., we consider extracellular magnetite precipitation by DIRB rather than intracellular controlled magnetite precipitation by MTB. Therefore, the different metabolic processes could affect the transfer of chemical elements from the external substrates to magnetite.

On the other hand, the presence of biomass and EPS could impact Zn and Ni partitioning. Total Organic Carbon (TOC) of biotic transformation products (5.1-9.3%) were higher than that of abiotic transformation products (0.3-1.8%) (Table S4). Therefore, in biotic experiments, Zn and Ni released from Fh by *S. oneidensis* MR-1 could adsorb onto cell surfaces or EPS and thus co-precipitated with biogenic magnetite (Tomaszewski et al., 2020), resulting in higher Zn and Ni partition coefficients in biogenic magnetite here than in Amor et al. (2015).

In principle, for magnetite precipitated in $NaHCO_3$ buffer, dissolution of siderite by the NaAc treatment could have released trace metals back into solution and then adsorbed on magnetite surfaces or re-precipitated, but no Zn or Ni mineralized components were detected by XRD, implying the amount of $ZnCO_3$ or $NiCO_3$ precipitated was either minor, or that they were X-ray amorphous. Although the Zn recovery for the abiotic transformation system for ZnFh (124-138%) was higher than 100%, for most setups, the Zn recovery for the biotic transformation products for ZnFh (104-110%) and Ni recovery for both abiotic and biotic transformation systems for NiFh (99-109%) were close to 100%, implying that potential contamination of NaAc was minor. Therefore, even if there was re-release of Zn and Ni by the NaAc treatment, this would not change our main conclusion since, compared with $NaHCO_3$ buffer, there were similar partitioning results for HEPES buffer in which there was in absence of dissolution of siderite.

4.4. Implications for the origin of magnetite in banded iron formations (BIF)

Konhauser et al. (2009) combined a compilation of Ni/Fe ratios in BIF with Ni partition coefficients for precipitated ferrihydrite to constrain the oceanic Ni reservoir through geological time, indicating a paleomarine Ni concentration of up to ~400 nM in the Archean, and a subsequent drop to ~200 nM by 2.5 Ga. In a similar manner, Robbins et al. (2013) measured Zn in BIFs and showed a relatively constant marine Zn reservoir through geological time, which is also in line with that of the black shale record (Scott et al., 2013). In the modern oceans, total dissolved Zn below the photic zone is 8–10 nM, where it remains relatively constant down to the seafloor (Bruland et al., 1994; Lohan et al., 2002). Combining the above estimates for Zn and Ni concentrations in Precambrian seawater and trace element data from magnetite grains from the c. 3.75 Ga old Nuvvuagittuq Supracrustal Belt in Québec (Canada), 2.45 Ga Weeli Wolli Iron Formation in Western Australia and 1.88 Ga Sokoman Iron Formation in the Labrador Trough (Canada) analyzed by laser ablation (Chung et al., 2015; Robbins et al., 2019), we reconstructed potential Zn and Ni partition coefficients between Precambrian seawater and magnetite grains in order to shed light on the origin of magnetite mineral grains within BIFs. As shown in Fig. 6, the ratios between reconstructed potential Zn and Ni partition coefficients for magnetite grains were >1, suggesting Zn was more enriched in these magnetite grains compared to Ni. Thus, we speculate that the magnetite grains in Nuvvuagittuq Supracrustal Belt, Weeli Wolli and Sokoman Iron Formation were abiogenic. These magnetite grains in these three formations could have formed through the reaction of settling ferrihydrite and Fe(II)-rich hydrothermal fluids that existed in the deeper waters (Li et al., 2017).

An alternative pathway for the abiogenic magnetite was ferrihydrite reduction by DIRB, where Fe(II) was transported to the ferrihydrite by diffusion or advection rather than in close proximity to the bacteria. In this scenario, there would be a disconnection between DIRB and the Zn and Ni scavenging processes. However, the organic carbon content in BIFs is extremely low and there is also no significant variation through time (Klein, 2005), suggesting that there was unlikely to have been more biomass production in the early Archean oceans than thereafter. In other words, the excess magnetite might not be a reflection of more organic carbon burial or enhanced DIRB but instead could have been due to the direct reaction of Fe^{2+} with ferric oxyhydroxides in seawater (Li et al., 2017). Moreover, negative δ^{56}Fe values are not found in the sedimentary record prior to around 2.9 Ga, Johnson et al. (2008) suggesting that DIRB did not have a large impact on the marine sedimentary record before that time. Therefore, the biogenic ori-

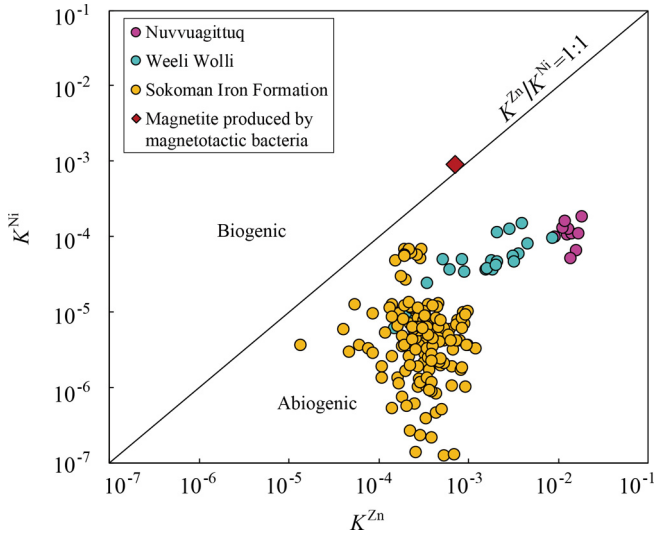

Fig. 6. Reconstructed Zn and Ni partition coefficients between Precambrian seawater and magnetite grains from the Nuvvuagittuq Supracrustal Belt, Québec, Canada (purple color), the Weeli Wolli Iron Formation in Western Australia (green color) and the Sokoman Iron Formation, Labrador Trough, Canada (orange color). The red diamond symbol represents the Zn and Ni partition coefficients for magnetite produced by magnetotactic bacteria in Amor et al. (2015).

gin (DIRB) of the Fe(II) could be available for the precipitation of magnetite grains in Weeli Wolli (2.45 Ga) and Sokoman Iron Formation (1.88 Ga), but not likely for Nuvvuagittuq Supracrustal Belt (3.75 Ga). Future studies should specifically focus on multi-trace elements in various minerals in BIFs to assess the applicability of trace element-partition coefficients on determining the biological or abiotic origin of minerals (e.g. siderite and magnetite) in BIFs. Additionally, some very negative δ^{56}Fe values for magnetite in BIFs may record DIRB as it is the most likely means to produce Fe^{2+}_{aq} with low δ^{56}Fe values in anoxic paleo-ocean (Johnson et al., 2008). Therefore, based on recent advancements in *in situ* trace element and Fe isotope measurements by laser ablation (LA) coupled to multi-collector–inductively coupled plasma–mass spectrometer (MC-ICP-MS), a multi-proxy approach combining trace element and Fe isotope characteristics is a promising tool to decipher the origin of magnetite in BIFs, particularly with respect to the abiogenic magnetite that derives from Fe(II) from a distal DIR source.

5. Conclusions

Overall, our data demonstrate that the Zn and Ni compositions in magnetite were highly dependent on the magnetite precipitation pathway (i.e., abiogenic transformation of ferrihydrite through reaction with dissolved Fe^{2+} from hydrothermal sources, or biogenic by ferrihydrite transformation by dissolved Fe^{2+} stemming from DIRB), regardless of whether the magnetite was precipitated in $NaHCO_3$ or HEPES buffer. The direct comparison of Zn and Ni partitioning in abiogenic and biogenic magnetite reveals that Zn was more enriched in abiogenic magnetite while Ni was more enriched in biogenic magnetite. We consider the different partitioning of Zn and Ni into abiogenic and biogenic magnetite could be related to differences in Fe(II)/Fe(III) ratio, coupled to the preference of Ni^{2+} ions to substitute for octahedral Fe^{2+} sites and Zn^{2+} ion preference for tetrahedral Fe^{3+} site substitution. Alternatively, if we consider the chemical composition of MTB magnetite, both Zn and Ni partition coefficients in biogenic magnetite reported in this study are much higher than that of MTB magnetite, which further supports the high chemical purity of MTB magnetite. The reconstructed Zn and Ni partition coefficients between Precambrian seawater and magnetite grains in BIFs could potentially serve as a geochemical constraint on the origin of magnetite grains within BIFs. However, caution must be exercised in predicting for the Zn and Ni concentrations of Precambrian oceans based on geochemical information recorded in a single mineral, because there are multiple minerals in BIFs. Further studies on various trace elements partitioning in iron-bearing minerals such as magnetite, hematite and siderite in BIFs are required to better understand and reconstruct on the origin of minerals in BIFs and the evolution of trace elements on the early Earth. A multi-proxy approach, such as a combination of trace elements and Fe isotope composition to decipher the origin of minerals in BIFs could be widely applied in the future.

CRediT authorship contribution statement

Xiaohua Han: Conceptualization, Methodology, Investigation, Writing, Validation, Visualization. **Elizabeth J. Tomaszewski:** Methodology, Writing. **Ronny Schoenberg:** Resources, Writing. **Kurt O. Konhauser:** Conceptualization, Writing. **Matthieu Amor:** Conceptualization, Writing. **Yongxin Pan:** Supervision, Writing. **Viola Warter:** Conceptualization, Writing. **Andreas Kappler:** Conceptualization, Supervision, Writing. **James M. Byrne:** Conceptualization, Supervision, Visualization, Writing.

Declaration of competing interest

The authors declare that they have no known competing financial interests or personal relationships that could have appeared to influence the work reported in this paper.

Acknowledgements

This research was funded by the German Research Foundation (DFG) under grant no. KA 1736/39-1. We would like to thank several people for their assistance and contributions to this manuscript. Ellen Röhm for assisting with TOC analyses, as well as general laboratory assistance, Natalia Jakus for XRD sample preparation and measurements, Bernd Steinhilber for trace elements analyses, Lars Grimm for assisting with bacteria incubation, Julian Sorwat and Manuel Schad for Mössbauer spectroscopy measurements and spectra fitting. Y.P. and X.H. were supported by a grant of the National Natural Science Foundation of China (41621004).

Appendix A. Supplementary material

Supplementary material related to this article can be found online at https://doi.org/10.1016/j.epsl.2021.117052.

References

Albut, G., Babechuk, M.G., Kleinhanns, I.C., Benger, M., Beukes, N.J., Steinhilber, B., Smith, A.J.B., Kruger, S.J., Schoenberg, R., 2018. Modern rather than Mesoarchaean oxidative weathering responsible for the heavy stable Cr isotopic signatures of the 2.95 Ga old Ijzermijn iron formation (South Africa). Geochim. Cosmochim. Acta 228, 157–189.

Althaus, E.W., Outten, C.E., Olson, K.E., Cao, H., O'Halloran, T.V., 1999. The ferric uptake regulation (Fur) repressor is a zinc metalloprotein. Biochemistry 38, 6559–6569.

Amor, M., Busigny, V., Duranddubief, M., Tharaud, M., Onanguema, G., Gélabert, A., Alphandéry, E., Menguy, N., Benedetti, M.F., Chebbi, I., 2015. Chemical signature of magnetotactic bacteria. Proc. Natl. Acad. Sci. USA 112, 1699–1703.

Amor, M., Mathon, F.P., Monteil, C.L., Busigny, V., Lefevre, C.T., 2020. Iron-biomineralizing organelle in magnetotactic bacteria: function, synthesis and preservation in ancient rock samples. Environ. Microbiol. 22, 3611–3632.

Bekker, A., Slack, J.F., Planavsky, N., Krapez, B., Hofmann, A., Konhauser, K.O., Rouxel, O.J., 2010. Iron formation: the sedimentary product of a complex interplay among mantle, tectonic, oceanic, and biospheric processes. Econ. Geol. 105, 467–508.

Bénézeth, P., Dandurand, J., Harrichoury, J.J.C.G., 2009. Solubility product of siderite (FeCO3) as a function of temperature (25–250 C). Chem. Geol. 265, 3–12.
Berthold, C., Bjeoumikhov, A., Brügemann, L., 2009. Fast XRD2 microdiffraction with focusing X-ray microlenses. Part. Part. Syst. Charact. 26, 107–111.
Blakemore, R., 1975. Magnetotactic bacteria. Science 190, 377.
Bruland, K.W., Orians, K.J., Cowen, J.P., 1994. Reactive trace metals in the stratified central North Pacific. Geochim. Cosmochim. Acta 58, 3171–3182.
Chung, D., Zhou, M.-F., Gao, J.-F., Chen, W.T., 2015. In-situ LA–ICP-MS trace elemental analyses of magnetite: the late Palaeoproterozoic Sokoman Iron Formation in the Labrador Trough, Canada. Ore Geol. Rev. 65, 917–928.
Coker, V.S., Pearce, C.I., Lang, C., van der Laan, G., Pattrick, R.A., Telling, N.D., Schüler, D., Arenholz, E., Lloyd, J.R., 2007. Cation site occupancy of biogenic magnetite compared to polygenic ferrite spinels determined by X-ray magnetic circular dichroism. Eur. J. Mineral. 19, 707–716.
Coker, V.S., Pearce, C.I., Pattrick, R.A.D., van der Laan, G., Telling, N.D., Charnock, J.M., Arenholz, E., Lloyd, J.R., 2008. Probing the site occupancies of Co-, Ni-, and Mn-substituted biogenic magnetite using XAS and XMCD. Am. Miner. 93, 1119–1132.
Cornell, R.M., Schwertmann, U., 2003. The Iron Oxides: Structure, Properties, Reactions, Occurrences and Uses. John Wiley & Sons.
Dippon, U., Schmidt, C., Behrens, S., Kappler, A., 2015. Secondary mineral formation during ferrihydrite reduction by Shewanella oneidensis MR-1 depends on incubation vessel orientation and resulting gradients of cells, Fe2+ and Fe minerals. Geomicrobiol. J. 32, 878–889.
Dupont, C.L., Butcher, A., Valas, R.E., Bourne, P.E., Caetano-Anollés, G., 2010. History of biological metal utilization inferred through phylogenomic analysis of protein structures. Proc. Natl. Acad. Sci. USA 107, 10567.
Dupuis, C., Beaudoin, G., 2011. Discriminant diagrams for iron oxide trace element fingerprinting of mineral deposit types. Miner. Depos. 46, 319–335.
Halama, M., Swanner, E.D., Konhauser, K.O., Kappler, A., 2016. Evaluation of siderite and magnetite formation in BIFs by pressure–temperature experiments of Fe(III) minerals and microbial biomass. Earth Planet. Sci. Lett. 450, 243–253.
Halevy, I., Alesker, M., Schuster, E.M., Popovitzbiro, R., Feldman, Y., 2017. A key role for green rust in the Precambrian oceans and the genesis of iron formations. Nat. Geosci. 10.
Han, X., Tomaszewski, E.J., Sorwat, J., Pan, Y., Kappler, A., Byrne, J.M., 2020a. Oxidation of green rust by anoxygenic phototrophic Fe(II)-oxidising bacteria. Geochem. Perspect. Lett. 12, 52–57.
Han, X., Tomaszewski, E.J., Sorwat, J., Pan, Y., Kappler, A., Byrne, J.M., 2020b. Effect of microbial biomass and humic acids on abiotic and biotic magnetite formation. Environ. Sci. Technol. 54, 4121–4130.
Hansel, C.M., Benner, S.G., Fendorf, S., 2005. Competing Fe (II)-induced mineralization pathways of ferrihydrite. Environ. Sci. Technol. 39, 7147–7153.
Hao, L., Guo, Y., Byrne, J.M., Zeitvogel, F., Schmid, G., Ingino, P., Li, J., Neu, T.R., Swanner, E.D., Kappler, A., 2016. Binding of heavy metal ions in aggregates of microbial cells, EPS and biogenic iron minerals measured in-situ using metal- and glycoconjugates-specific fluorophores. Geochim. Cosmochim. Acta 180, 66–96.
Johnson, C.M., Beard, B.L., Beukes, N.J., Klein, C., O'Leary, J.M., 2003. Ancient geochemical cycling in the Earth as inferred from Fe isotope studies of banded iron formations from the Transvaal Craton. Contrib. Mineral. Petrol. 144, 523–547.
Johnson, C.M., Roden, E.E., Welch, S.A., Beard, B.L., 2005. Experimental constraints on Fe isotope fractionation during magnetite and Fe carbonate formation coupled to dissimilatory hydrous ferric oxide reduction. Geochim. Cosmochim. Acta 69, 963–993.
Johnson, C.M., Beard, B.L., Roden, E.E., 2008. The iron isotope fingerprints of redox and biogeochemical cycling in modern and ancient Earth. Annu. Rev. Earth Planet. Sci. 36, 457–493.
Jolivet, J.P., Belleville, P., Tronc, E., Livage, J., 1992. Influence of Fe(II) on the formation of the spinel iron oxide in alkaline medium. Clays Clay Miner. 40, 531–539.
Klein, C., 2005. Some Precambrian banded iron-formations (BIFs) from around the world: their age, geologic setting, mineralogy, metamorphism, geochemistry, and origins. Am. Miner. 90, 1473.
Kohler, I., Konhauser, K.O., Papineau, D., Bekker, A., Kappler, A., 2013. Biological carbon precursor to diagenetic siderite with spherical structures in iron formations. Nat. Commun. 4, 7.
Konhauser, K.O., Newman, D.K., Kappler, A., 2005. The potential significance of microbial Fe(III) reduction during deposition of Precambrian banded iron formations. Geobiology 3, 167–177.
Konhauser, K.O., Amskold, L., Lalonde, S.V., Posth, N.R., Kappler, A., Anbar, A., 2007. Decoupling photochemical Fe(II) oxidation from shallow-water BIF deposition. Earth Planet. Sci. Lett. 258, 87–100.
Konhauser, K.O., Pecoits, E., Lalonde, S.V., Papineau, D., Nisbet, E.G., Barley, M.E., Arndt, N.T., Zahnle, K., Kamber, B.S., 2009. Oceanic nickel depletion and a methanogen famine before the Great Oxidation Event. Nature 458, 750.
Konhauser, K.O., Planavsky, N.J., Hardisty, D.S., Robbins, L.J., Warchola, T.J., Haugaard, R., Lalonde, S.V., Partin, C.A., Oonk, P.B.H., Tsikos, H., Lyons, T.W., Bekker, A., Johnson, C.M., 2017. Iron formations: a global record of Neoarchaean to Palaeoproterozoic environmental history. Earth-Sci. Rev. 172, 140–177.
Li, Y.-L., Konhauser, K.O., Cole, D.R., Phelps, T.J., 2011. Mineral ecophysiological data provide growing evidence for microbial activity in banded-iron formations. Geology 39, 707–710.
Li, Y.L., Konhauser, K.O., Zhai, M., 2017. The formation of magnetite in the early Archean oceans. Earth Planet. Sci. Lett. 466, 103–114.
Lies, D.P., Hernandez, M.E., Kappler, A., Mielke, R.E., Gralnick, J.A., Newman, D.K., 2005. Shewanella oneidensis MR-1 uses overlapping pathways for iron reduction at a distance and by direct contact under conditions relevant for biofilms. Appl. Environ. Microbiol. 71, 4414.
Lohan, M.C., Statham, P.J., Crawford, D.W., 2002. Total dissolved zinc in the upper water column of the subarctic North East Pacific. Deep-Sea Res., Part 2, Top. Stud. Oceanogr. 49, 5793–5808.
Mulrooney, S.B., Hausinger, R.P., 2003. Nickel uptake and utilization by microorganisms. FEMS Microbiol. Rev. 27, 239–261.
Nadoll, P., Angerer, T., Mauk, J.L., French, D., Walshe, J., 2014. The chemistry of hydrothermal magnetite: a review. Ore Geol. Rev. 61, 1–32.
Ohmoto, H., Watanabe, Y., Kumazawa, K., 2004. Evidence from massive siderite beds for a CO2-rich atmosphere before ∼ 1.8 billion years ago. Nature 429, 395–399.
Piepenbrock, A., Dippon, U., Porsch, K., Appel, E., Kappler, A., 2011. Dependence of microbial magnetite formation on humic substance and ferrihydrite concentrations. Geochim. Cosmochim. Acta 75, 6844–6858.
Porsch, K., Kappler, A., 2011. FeII oxidation by molecular O2 during HCl extraction. Environ. Chem. 8, 190–197.
Posth, N.R., Köhler, I., Swanner, E.D., Schröder, C., Wellmann, E., Binder, B., Konhauser, K.O., Neumann, U., Berthold, C., Nowak, M., Kappler, A., 2013b. Simulating Precambrian banded iron formation diagenesis. Chem. Geol. 362, 66–73.
Posth, N.R., Konhauser, K.O., Kappler, A., 2013a. Microbiological processes in banded iron formation deposition. Sedimentology 60, 1733–1754.
Posth, N.R., Canfield, D.E., Kappler, A., 2014. Biogenic Fe(III) minerals: from formation to diagenesis and preservation in the rock record. Earth-Sci. Rev. 135, 103–121.
Rancourt, D.G., Ping, J.Y., 1991. Voigt-based methods for arbitrary-shape static hyperfine parameter distributions in Mössbauer spectroscopy. Nucl. Instrum. Methods Phys. Res. B 58, 85–97.
Rasmussen, B., Muhling, J.R., 2018. Making magnetite late again: evidence for widespread magnetite growth by thermal decomposition of siderite in Hamersley banded iron formations. Precambrian Res. 306, 64–93.
Rasmussen, B., Muhling, J.R., Suvorova, A., Krapež, B., 2017. Greenalite precipitation linked to the deposition of banded iron formations downslope from a late Archean carbonate platform. Precambrian Res. 290, 49–62.
Raven, K.P., Jain, A., Loeppert, R.H., 1998. Arsenite and arsenate adsorption on ferrihydrite: kinetics, equilibrium, and adsorption envelopes. Environ. Sci. Technol. 32, 344–349.
Robbins, L.J., Lalonde, S.V., Saito, M.A., Planavsky, N.J., Mloszewska, A.M., Pecoits, E., Scott, C., Dupont, C.L., Kappler, A., Konhauser, K.O., 2013. Authigenic iron oxide proxies for marine zinc over geological time and implications for eukaryotic metallome evolution. Geobiology 11, 295–306.
Robbins, L.J., Konhauser, K.O., Warchola, T.J., Homann, M., Thoby, M., Foster, I., Mloszewska, A.M., Alessi, D.S., Lalonde, S.V., 2019. A comparison of bulk versus laser ablation trace element analyses in banded iron formations: insights into the mechanisms leading to compositional variability. Chem. Geol. 506, 197–224.
Schiessl, W., Potzel, W., Karzel, H., Steiner, M., Kalvius, G., Martin, A., Krause, M., Halevy, I., Gal, J., Schäfer, W., et al., 1996. Magnetic properties of the ZnFe2O4 spinel. Phys. Rev. B 53, 9143.
Scott, C., Planavsky, N.J., Dupont, C.L., Kendall, B., Gill, B.C., Robbins, L.J., Husband, K.F., Arnold, G.L., Wing, B.A., Poulton, S.W., Bekker, A., Anbar, A.D., Konhauser, K.O., Lyons, T.W., 2013. Bioavailability of zinc in marine systems through time. Nat. Geosci. 6, 125–128.
Stookey, L.L., 1970. Ferrozine—a new spectrophotometric reagent for iron. Anal. Chem. 42, 779–781.
Sun, S., Konhauser, K.O., Kappler, A., Li, Y.-L., 2015. Primary hematite in Neoarchean to Paleoproterozoic oceans. Geol. Soc. Am. Bull. 127, 850–861.
Tomaszewski, E.J., Olson, L., Obst, M., Byrne, J.M., Kappler, A., Muehe, E.M., 2020. Complexation by cysteine and iron mineral adsorption limit cadmium mobility during metabolic activity of Geobacter sulfurreducens. Environ. Sci. Process Impacts 22, 1877–1887.
van Zuilen, M.A., Lepland, A., Arrhenius, G., 2002. Reassessing the evidence for the earliest traces of life. Nature 418, 627–630.
Vargas, M., Kashefi, K., Blunt-Harris, E.L., Lovley, D.R., 1998. Microbiological evidence for Fe(III) reduction on early Earth. Nature 395, 65–67.
Xiao, W., Jones, A.M., Li, X., Collins, R.N., Waite, T.D., 2018. Effect of Shewanella oneidensis on the kinetics of Fe(II)-catalyzed transformation of ferrihydrite to crystalline iron oxides. Environ. Sci. Technol. 52, 114–123.
Zerkle, A.L., House, C.H., Brantley, S.L., 2005. Biogeochemical signatures through time as inferred from whole microbial genomes. Am. J. Sci. 305, 467–502.